Bulletin of the Institute of Mathematics
Academia Sinica (New Series)
Vol. **3** (2008), No. 4, pp. 585-601

A NESTED SEQUENCE OF TRANSITIONS FOR COLLISION DYNAMICS IN DISSIPATIVE SYSTEMS

BY

Masaaki Yadome, Kei-Ichi Ueda, Takashi Teramoto,
Masaharu Nagayama and Yasumasa Nishiura

Dedicated to Professor Masayasu Mimura on his 65th birthday

Abstract

We study the dynamics of head-on collisions of traveling pulses for a three-component reaction diffusion system. A variety of outputs with large deformation such as annihilation, repulsion, and fusion are observed after collision, however it remains open for a long time that what kind of mathematical structure controls the input-output relation at collision point. A series of works [18, 19, 20, 24] clarify some aspect of scattering dynamics that a network of unstable patterns called *scattors* forms a backbone of the traffic control of input-output relations. Namely the unstable manifolds of those scattors constitute a network and complicated deformation processes and their transitions are controlled by rewiring those connections depending on parameters. In this article, by employing a three-component reaction diffusion system, we numerically show that there occurs a nested sequence of outputs among annihilation, repulsion, and fusion as parameters are varied in an appropriate way. It turns out that there exists a time-periodic unstable solution that plays a role of scattor and two heteroclinic connections are detected between the unstable periodic solution and other unstable stationary scattors which are responsible for the nested output of periodic type.

Received August 12, 2008.

AMS Subject Classification: 37M05 37M20 65P30.

Key words and phrases: Reaction-diffusion systems, pattern formation, pulse dynamics, bifurcation.

1. Introduction

Localized patterns such as traveling pulses and spots are the representative patterns in reaction-diffusion systems and are observed experimentally and numerically, for instance, in gas-discharge systems, CO oxidation processes, and various chemical reactions ([6, 11, 14, 17]). One of the interesting phenomena is the transient dynamics through intrinsic instability, such as the creation and destruction of localized patterns, for example, in self-replicating patterns [12, 21], spatio-temporal chaos [4, 22], localized spots [3, 5, 23], and so on. It is known that intrinsic instabilities and strong interactions between these patterns cause the emergence of more complex and dynamic patterns, for instance, self-similar patterns [10] and complex patterns [15]. The dynamics of interaction between two localized patterns gives a fundamental information for the understanding of such transient dynamics.

In recent years, several rigorous approaches to interaction dynamics have been proposed. A rigorous method for weakly interacting pulses have been proposed [7, 8], and is applied to the collision dynamics between two slowly propagating traveling pulses and allows us to reduce to finite dimensional ODEs. A challenge is to understand the real strong interaction between localized patterns with large deformation, which is still uncultivated area except for a scalar bistable reaction-diffusion equation for colliding fronts [16, 25] in which annihilation process was clarified by using comparison arguments. A variety of outputs are produced after strong interaction including fusion and repulsion for a large class of reaction diffusion systems. In order to understand strong interaction dynamics, a computer-aided analysis is quite useful. Argentina et al. predicted that, in some dissipative systems, output patterns after head-on collisions between two localized patterns are described by the global behavior of the unstable manifold of the separator [1, 2]. More systematically Nishiura et al. showed that a network consisting of unstable solutions and their unstable manifolds control the collision dynamics; the solution orbit approaches an unstable solution called *scattor*, and the change of final output is governed by the basin-switching of the orbit as parameters vary [18, 19, 20, 24]. These observations indicate that the final output after a head-on collision is controlled by the global behavior of the unstable manifolds of the scattors.

In this article, we consider the output patterns after a symmetric head-on collision in the following three-component reaction diffusion system:

$$\begin{aligned} u_t &= D_u u_{xx} - \frac{uv^2}{1+k_3 w} + k_2(1-u), \\ \tau v_t &= D_v v_{xx} + \frac{uv^2}{1+k_3 w} - (k_1+k_2)v, \qquad t \geq 0, \quad x \in [-L, L], \\ \theta w_t &= D_w w_{xx} + k_4(v-w), \end{aligned} \tag{1}$$

where $u = u(t,x), v = v(t,x), w = w(t,x), D_u = 5.0 \times 10^{-5}, D_v = 3.0 \times 10^{-5}, D_w = 4.0 \times 10^{-5}, k_2 = 0.032, k_3 = 1.0, k_4 = 0.01, \theta = 5.0$, and $L = 1.0$. One of the interesting phenomena in (1) is the existence of nested transition sequences of output patterns after head-on collisions. As shown in Fig. 1, the annihilation and fusion patterns appear densely, and the output pattern changes sensitively depending on the parameter values near the boundary of the repulsion region. Furthermore, we can find small repulsion regions between the annihilation and fusion regions. The purpose of this article is to clarify how such output pattern sequences appear and predict the exact sequence.

In [20], by performing careful numerical experiments with respect to the system (1), it has been clarified that the orbit comes sufficiently close to the heteroclinic orbit connecting two scattors by taking parameter values close to a triple junction where the boundaries of the annihilation, repulsion, and fusion regions are in contact. That is, the solution orbits after head-on collisions are sorted by more than two scattors near the triple junction. However, in their numerical results, no nested sequences including annihilation and fusion regions have been observed.

In this article, in order to clarify how nested output sequences and small repulsion regions appear, we numerically showed that there exist three unstable solutions (one periodic solution and two stationary solutions), and the heteroclinic orbits connecting them are responsible for the sequence.

This article is organized as follows. In Section 2, we show the phase diagrams of the output patterns after head-on collisions, and find the parameters associated with the onset of the nested sequence. In Section 3, we numerically detect a scattor near the onset of a nested sequence, and

consider how the output sequence appears by investigating the dynamical behavior of the unstable manifolds emanating from the scattor.

2. Phase Diagram and Bifurcation Diagram

The system in (1) is the same as that in the Gray-Scott model [9] if w is ignored, i.e., for $k_3 = 0$. The variable w is an inhibitor of the production of u. In this article, we consider the symmetric head-on collision between two traveling pulses. Therefore, in the numerical simulation, we investigate the output patterns after collision with a Neumann (no-flux) wall. The initial data is taken to be close to a stable traveling pulse solution, and k_1 and τ are taken as control parameters.

The phase diagram of the outputs is shown in Fig. 1. Taking $\tau = 1.21$ and increasing k_1 from the repulsion region of the leftmost side, the nested sequence of the fusion and annihilation patterns can be observed as shown in Fig. 1. The width of the stripes increases as k_1 increases. Investigating the sequence more carefully, two small repulsion regions are observed (R(11) and R(13) in Fig. 1(c)). That is, as precisely as possible by using a numerical method, the sequence changes as R(1)→A(2)→F(3)→A(4)→F(5)→A(6)→F(7)→A(8)→F(9)→A(10)→R(11) →F(12)→R(13)→A(14), where A, R, and F are abbreviations of annihilation, repulsion, and fusion, respectively.

It is convenient to show the global bifurcation diagram of pulse solution in order to consider the origin of the transitions of output patterns (see [18]). Figure 2 shows the global bifurcation diagram of a half-pulse solution located at a boundary wall for $\tau = 1.21$. The branches of the periodic solution are detected by using the shooting method [13]. We note that the existence region of the branch in the bifurcation diagram is equivalent to a symmetric single pulse solution when the domain size is twice as large as that of this system. Bifurcation points of asymmetric instabilities of single-pulse solutions, such as drift instability, are depressed for half-pulse solutions, and therefore no branches of the traveling pulse and the traveling breathers exist in the diagram. The upper branch in Fig. 2, corresponding to a stationary pulse solution, bifurcates from the stationary steady state, and the amplitude of the pulse increases as k_1 increases. The pulse solution generates a saddle-node (SN) bifurcation at $k_1 \approx 0.057555$ (SN_1) and a second SN bifurcation at $k_1 \approx 0.051059$(SN_2). After SN_2, the depth of the dimple of the pulse

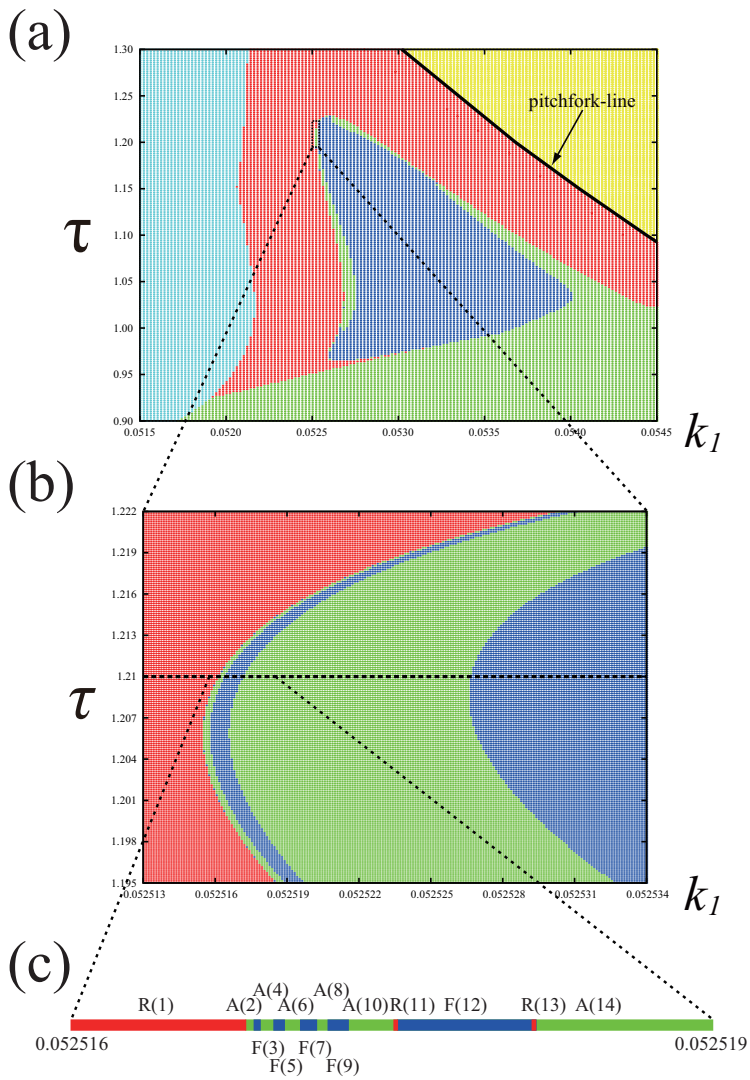

Figure 1. (a) Phase diagram after a symmetric head-on collision. Red: Repulsion. Green: Annihilation. Blue: Fusion. Yellow: Stable standing pulse. Light blue: Splitting. The solid line indicates the pitchfork bifurcation line. The traveling pulse solution bifurcates subcritically from stable standing pulse solution and recovers its stability by saddle-node bifurcation. Stable traveling pulse solutions exist in red, green, and blue regions. (b) The magnified figure of the dashed box in (a). (c) A schematic figure of the phase diagram for $\tau = 1.21$. A nested sequence of annihilation and fusion is observed near the boundary of R(1). Small repulsion regions (R(11) and R(13)) are found between A(10) and F(12), and F(12) and A(14), respectively.

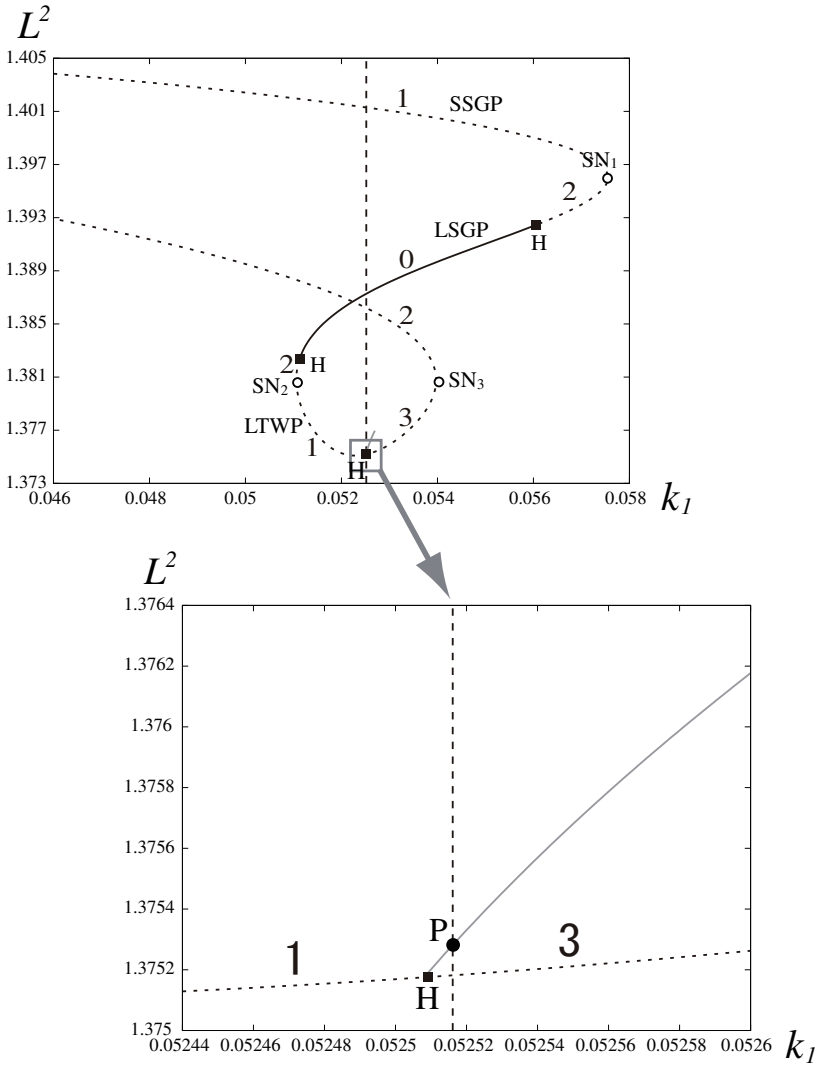

Figure 2. Bifurcation diagram of a half-pulse solution for $\tau = 1.21$. The solid (dotted) line indicates stable (unstable) stationary solutions, and the gray line indicates periodic solutions. Also, H and SN_j $(j = 1, 2, 3)$ indicate Hopf and saddle-node bifurcation points, respectively. Furthermore, the number in the diagram denotes the number of unstable eigenvalues, and the vertical dashed line is $k_1 \approx 0.052516$, where nested sequence appears.

increases as k_1 increases. The amplitude of the pulse decreases after the SN bifurcation $k_1 \approx 0.053969$ (SN_3). We refer to the stationary single pulse solution as SSGP (small single-horn pulse) before SN_1, as LSGP (large single-

horn pulse) between SN_1 and SN_2, and as LTWP (large twin-horn pulse) between SN_2 and SN_3. Since the profile is independent of time constant τ, we consistently use the same notations for any τ in this article.

3. Global Connections between Scattors

It has been numerically shown that an unstable solution referred to as scattor plays the role of a traffic controller of the solution orbit near the transition point ([18, 19, 20]). That is, the final destination of the solution is characterized by the behavior of the unstable manifold emanating from the scattor. In this section, in order to clarify the mechanism of emergence of the nested sequences A and F, as well as that of the small repulsion regions which are observed between A(10) and A(14), we numerically find the scattors and investigate how the solution orbits are sorted around the scattors.

First, we consider how the nested sequence emerges from the boundary of the right side of R(1). In order to find a scattor responsible for the emergence of a nested sequence, we take the parameter near the boundary and investigate the scattering dynamics near the boundary, which is shown in Fig. 3. It is numerically confirmed that the solution orbit comes closer and closer to the periodic solution as k_1 is taken closer to the boundary. The periodic solution, for example, $P(t, x)$, coincides with the one which emanates from the Hopf bifurcation point of LTWP (Fig. 2). The unstable oscillatory standing pulse P has one unstable mode, i.e., the monodromy matrix of P has a Floquet multiplier $\lambda_1 \approx 50.95 > 1$. The profile of the snapshot of P and that of the eigenfunction $\Phi(x)$ corresponding to λ_1 is shown in Fig. 4(a). Next, we add a small perturbation to scattor P and observe the output patterns and their phase dependency. That is, the initial data $\widetilde{P}(x)$ is taken as follows:

$$\widetilde{P}(x) = P(0, x) + \epsilon_0 \Phi(x), \tag{2}$$

where $\epsilon_0 \in \mathbf{R}$ takes a small value. Figure 4 shows the output pattern sequence when ϵ_0 is varied, where a nested sequence of fusion or annihilation is observed for $\epsilon_0 > 0$, and repulsion is observed for $\epsilon_0 < 0$. This result indicates that the determination of the solution is strongly sensitive with respect to changes, depending on its phase of oscillation when the solution

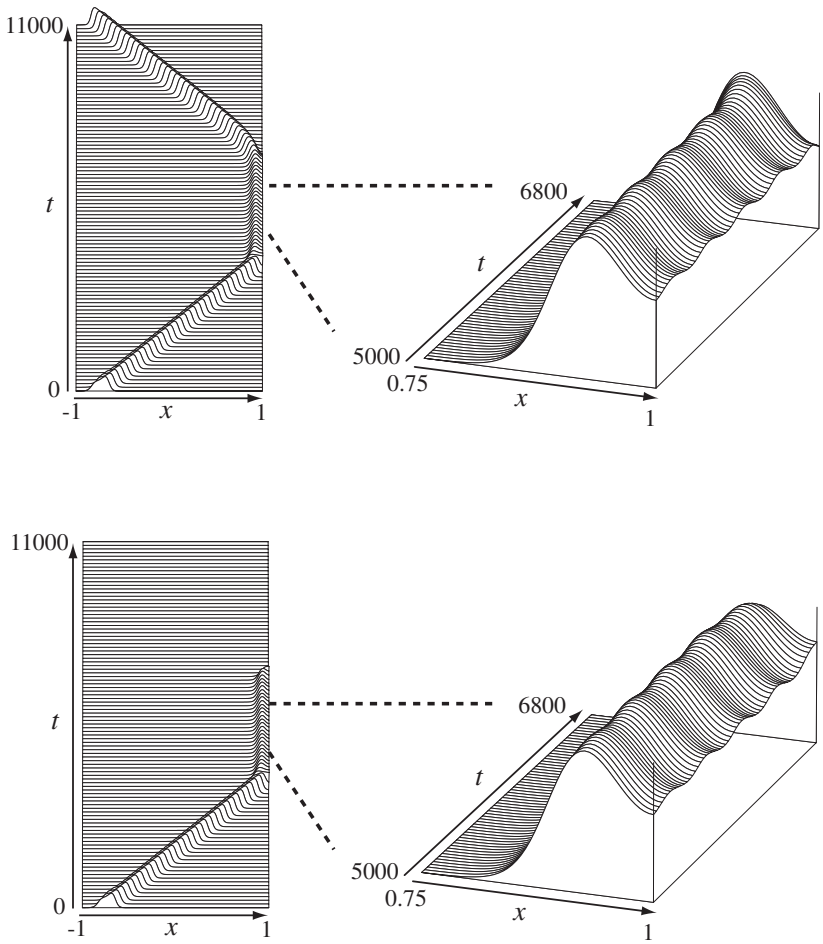

Figure 3. Bird's-eye view of the pulse dynamics near the boundary of R(1). The solution orbit comes closer and closer to a periodic solution as k_1 is taken closer to the boundary of R(1). Only the v-component is displayed.

approaches P. Furthermore, since an unstable manifold emanating from P leaves by winding around it, it is found that the output pattern changes periodically by selecting larger values for ϵ_0 (Fig. 5), and the winding number around P before the solution goes to the final destination decreases as the initial data is taken far from P, i.e., when ϵ_0 is large. It should be noted that the winding number also decreases as k_1 is taken far from the boundary of R(1) (Fig. 6), which suggests that the origin of the nested sequence is dependent on the flows of the unstable manifold.

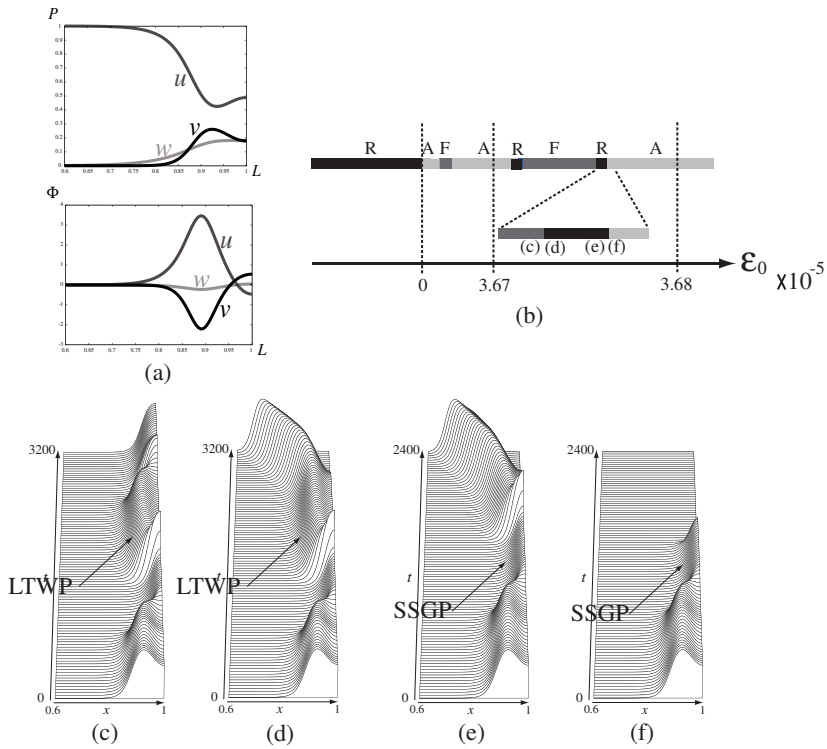

Figure 4. (a) A snapshot of P and the eigenfunction Φ corresponding to λ_1. (b) A schematic phase diagram of the output patterns for small perturbations of Φ to P. (c)(d) [(e)(f)] Dynamic behavior when a small perturbation is applied to P near the point marking the transition from F to R [from R to A] in (b). It is observed that the solution orbit approaches LTWP (large twin-horn pulse) [SSGP (small single-horn pulse)] before it arrives at the final destination.

Next, we consider how small repulsion regions appear between A(10) and F(12) and between F(12) and A(14). Hereafter, we focus exclusively on the transition from F(12) to A(14) since the transition from A(10) to F(12) can be described by using parallel arguments.

Now, we observe the scattering dynamics near the transition points between R(13) and A(14) and between F(12) and R(13). By taking the parameter value close to the transition point between R(13) and A(14), it is observed that the solution orbit approaches P and then SSGP after colliding with the boundary wall. Also, the solution orbit approaches P and then

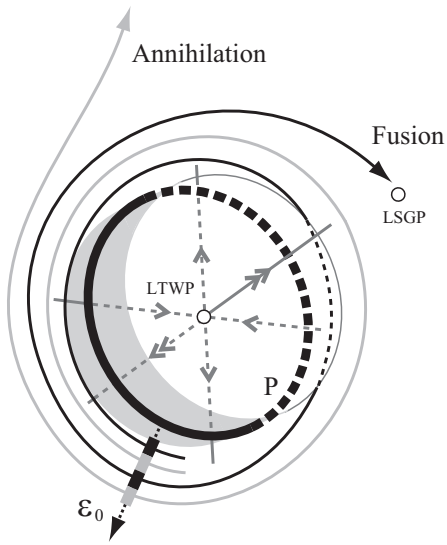

Figure 5. A schematic figure of the orbital behavior of an unstable manifold corresponding to the scattor P. Since an unstable manifold emanating from the scattor leaves it by winding around it, the output changes periodically by changing the initial position transversally to the flow of the unstable manifold. When the initial data is taken by varying ϵ_0, the output pattern changes periodically.

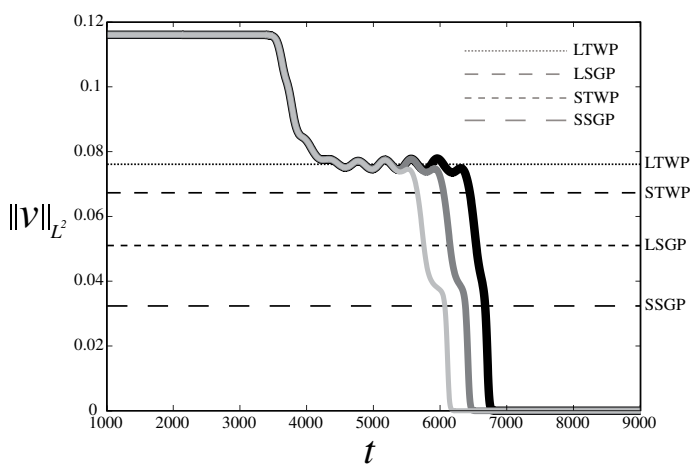

Figure 6. Time series of the solution orbit near R(1). Since the solution orbit comes closer to P by taking k_1 closer to the boundary of R(1), the winding number around P decreases as k_1 goes far from the boundary. The black, dark gray, and gray lines show the time sequence when the parameter value is taken from region A(4), A(6), and A(8), respectively.

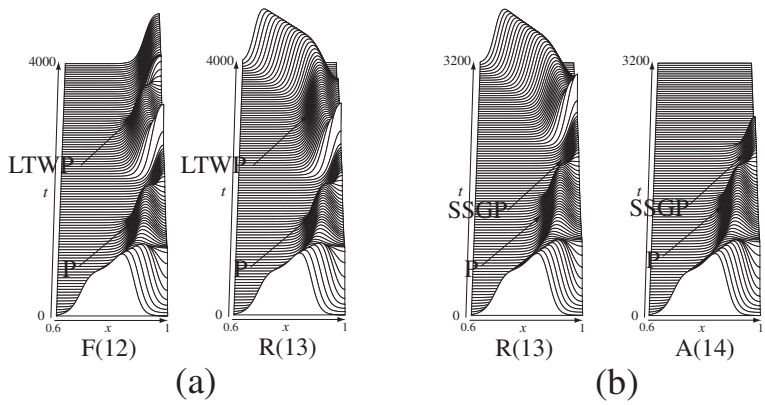

Figure 7. (a) [(b)] Pulse dynamics near the point marking the transition from F(12) to R(13) [from R(13) to A(14)]. The solution orbit approaches P and LTWP (large twin-horn pulse) [P and SSGP (small single-horn pulse)] after a collision.

LTWP when k_1 is taken near the transition point between F(12) and R(13) (Fig. 7). From these observations, we can predict that final destinations change when the solution orbit crosses the separatrix (the stable manifold) of SSGP and LTWP, and their unstable manifold are responsible for the final destinations. Furthermore, we can predict the existence of two types of heteroclinic orbits, one connecting P and SSGP, and the other one connecting P and LTWP.

We show that the destinations of the unstable manifolds of the SSGP are in fact repulsion and annihilation. The unstable solution has one positive eigenvalue $\lambda_1^1 \approx 0.0519$, and the profile of the eigenfunction ϕ_1^1 is shown in Fig. 8(a). The behavior of the unstable manifold corresponding to λ_1^1 is confirmed by adding a small perturbation to the unstable solution, i.e., the initial data $\widetilde{S}_{\mathrm{SSGP}}$ is taken as follows:

$$\widetilde{S}_{\mathrm{SSGP}} = S_{\mathrm{SSGP}} + \epsilon_1 \phi_1^1, \tag{3}$$

where S_{SSGP} is the SSGP for the transition point between R(13) and A(14), and $\epsilon_1 \in \mathbf{R}$ has a small value. It is observed that, as shown in Fig. 8(b), the outputs are annihilation and repulsion depending on the sign of ϵ_1, i.e., the destinations of the unstable manifold are repulsion and annihilation.

Similarly, we investigate the behavior of unstable manifolds corresponding to the LTWP. The unstable solution has three unstable eigenvalues, which consist of one positive real $\lambda_1^2 = 0.010$ and one complex pair $\lambda_2^2 =$

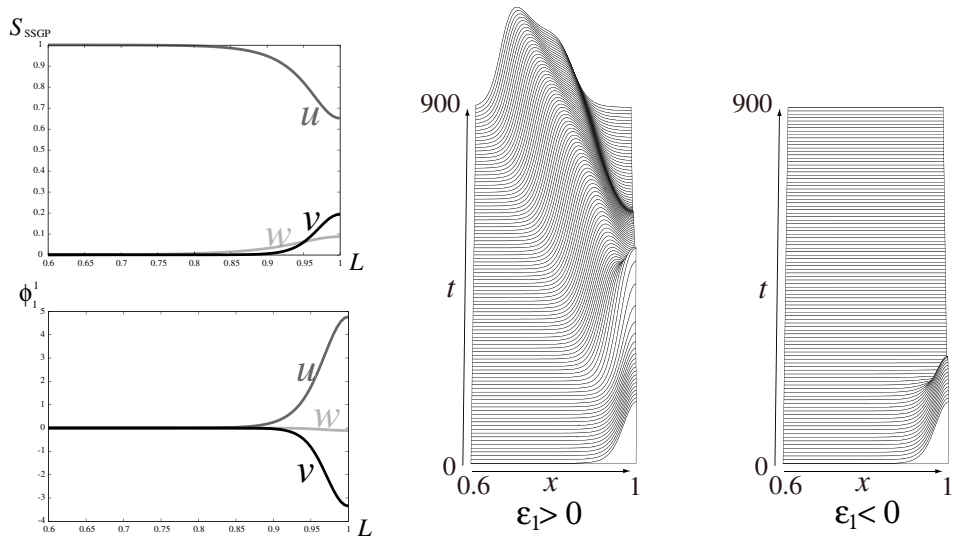

Figure 8. (a) The respective profiles of S_{SSGP} and ϕ_1^1. (b) The output patterns for a small perturbation of ϕ_1 to S_{SSGP}. Repulsion and annihilation is observed for negative and positive ϵ_1, respectively.

$4.91 \times 10^{-5} \pm 0.016i$. Since the real part of λ_2^2 is much smaller than λ_1^2, we can ignore the unstable direction corresponding to λ_2^2, and therefore we investigate the output patterns by taking the initial data $\widetilde{S}_{\mathrm{LTWP}}$ as follows:

$$\widetilde{S}_{\mathrm{LTWP}} = S_{\mathrm{LTWP}} + \epsilon_2 \phi_1^2, \tag{4}$$

where S_{LTWP} is the LTWP for the transition point between F(12) and R(13), and $\epsilon_2 \in \mathbf{R}$ takes a small value and ϕ_1^2 is an unstable eigenfunction corresponding to λ_1^2. The profile of ϕ_2^1 is shown in Fig. 9(a). Repulsion and fusion dynamics is observed for positive and negative ϵ_2, respectively. That is, the output pattern is repulsion or fusion depending on which side of the unstable manifold the solution orbit belongs to (Fig. 9(b)). From these experiments, we find that small repulsion regions emerge when the solution orbit crosses the stable manifold of SSGP or LTWP.

By performing similar numerical experiments, we can confirm that the solution orbit approaches SSGP and LTWP near the transition point between A(10) and R(11) and that between R(11) and F(12), respectively. Also, the output pattern changes when the orbit crosses the stable manifold of SSGP or LTWP.

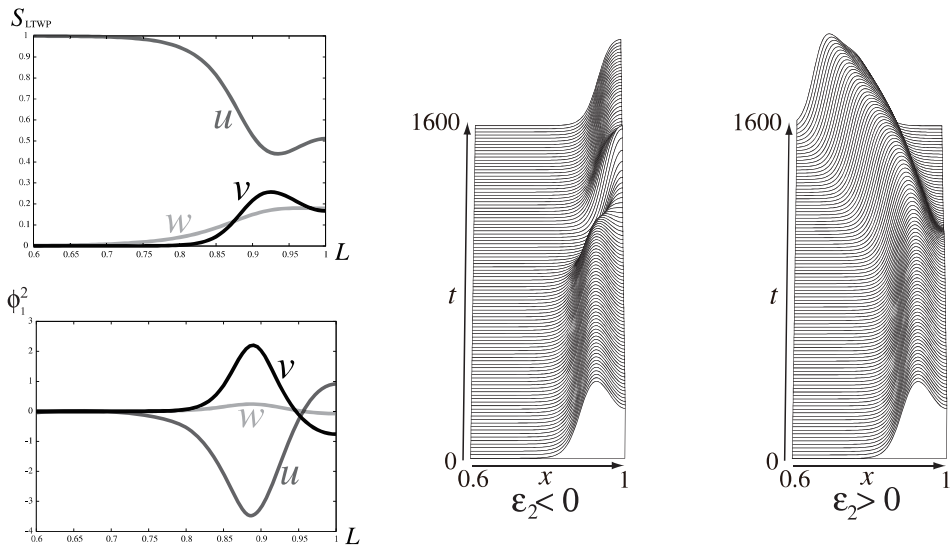

(a) (b)

Figure 9. (a) The respective profiles of S_{LTWP} and ϕ_1^2. (b) The output patterns for a small perturbation of ϕ_1^2 to S_{LTWP}. Fusion and annihilation is observed for negative and positive ϵ_2, respectively.

We show that the origin of the output pattern sequence A→R→F→R→A is described by the global behavior of the unstable manifold of P. In this case, small perturbations of Φ are applied again to P, and the output patterns are carefully observed for $\epsilon_0 \in [3.67 \times 10^{-5}, 3.68 \times 10^{-5}]$, where two annihilation regions and one fusion region are observed (Fig. 4). As shown in Fig. 4, it is clear that two small repulsion regions exist between the annihilation and fusion regions, i.e., the following transition sequence A→R→F→R→A is observed by varying ϵ_0 (see Fig. 10). Furthermore, the global behavior near the points marking the transition from A to R (from R to A), and the points marking the transition from R to F (from F to R) are qualitatively the same as those shown in scattering dynamics (Fig. 7). Therefore, it has been numerically confirmed that the sequence A→R→F→R→A shown in Fig. 1 is again observed by varying the position of the initial data continuously on the unstable manifold, which indicates that P is a scattor responsible for the transitions.

Finally, we predict the exact sequence near the boundary of R(1). In the previous paragraph, we showed that small repulsion regions appear between A and F. Also, as shown in Fig. 5, the region A and F appear periodically

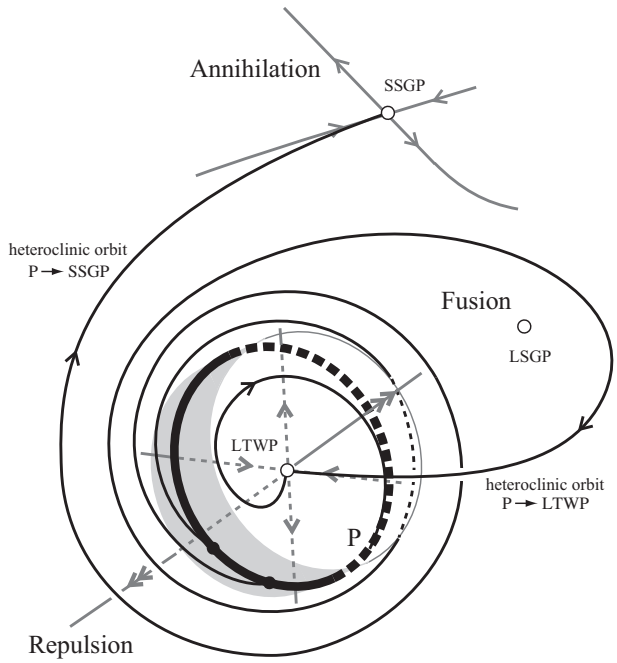

Figure 10. Flow chart of the solution orbits when the initial data is taken close to P. The output pattern changes when the solution orbit crosses the stable manifold of SSGP (small single-horn pulse) or LTWP (large twin-horn pulse), and two heteroclinic orbits are found at the transition points.

and densely near R(1). These results strongly suggest that small repulsion regions can be observed arbitrarily close to R(1), and infinite periodic sequence $\cdots$A$\to$R$\to$F$\to$R$\to$A$\to\cdots$ exists at the right side of R(1).

4. Summary

In this article, we observed nested output pattern sequences and small repulsion regions between annihilation and fusion regions. We found that the unstable oscillatory standing pulse P is a scattor which is responsible for such transitions. Although the unstable dimension of P is one, three types of output, namely annihilation, repulsion, and fusion, are observed as determinations of unstable manifold corresponding to P. In other words, the output patterns after a head-on collision become highly sensitive when the solution orbit comes close to P. In fact, we found that the changes in

the output patterns show high sensitivity toward the orbit, as indicated in the sequence from A(10) to A(14).

As discussed in Section 3, it is expected that, when the scattor is a periodic solution, periodic sequences exist densely near R(1), and small repulsion regions exist between each two adjacent A and F regions , i.e., the sequence $\cdots$ A$\rightarrow$ R$\rightarrow$F$\rightarrow$ R $\rightarrow$ A$\rightarrow$ $\cdots$ can be observed arbitrarily close to R(1). However, since the changes in the output patterns become more sensitive as k_1 approaches R(1), we can find small repulsion regions only between A(10) and A(14) due to the difficulties presented by the limited numerical precision. More precise numerical experiments using multiple precision floating-point numbers are needed in order to find such sequences in the neighborhood of R(1).

Acknowledgments

This research was partially supported by Grant-in-Aid for Young Scientists(A) 18684002 (to M.N.), Exploratory Research 19654017 (to M.N.), Young Scientists(B) 20740055 (to K.U.), and Young Scientists(B) 20740224 (to T.T.) from MEXT of Japan.

References

1. M. Argentina, P. Coullet and V. Krinsky, Head-on collisions of waves in an excitable FitzHugh–Nagumo system: a transition from wave annihilation to classical wave behavior, *J. Theo. Biol.*, **205** (2000), 47-52.

2. M. Argentina, P. Coullet and L. Mahadevan, Colliding waves in a model excitable medium: preservation, annihilation, and bifurcation, *Phys. Rev. Lett.*, **79** (1997), 2803-2806.

3. Y. A. Astrov and H.-G. Purwins, Plasma spots in a gas discharge system: birth, scattering and formation of molecules, *Phys. Lett. A*, **283** (2001), 349-354.

4. M. Bär, M. Eiswirth, H.-H. Rotermund and G. Ertl, Solitary-wave phenomena in an excitable surface reaction, *Phys. Rev. Lett.* **69** (1992), 945-948.

5. M. Bode, A. W. Liehra, C. P. Schenk and H.-G. Purwins, Interaction of dissipative solitons: particle-like behaviour of localized structures in a three-component reaction-diffusion system, *Physica D*, **161** (2002), 45-66.

6. P. de Kepper, J.-J. Perraud, B. Rudovics and E. Dulos, Experimental study of stationary Turing patterns and their interaction with traveling waves in a chemical system, *Int. J. Bifurcation Chaos Appl. Sci. Eng.*, **4** (1994), 1215-1231.

7. S. -I. Ei, The motion of weakly interacting pulses in reaction-diffusion systems, *J. Dyn. Diff. Eqs.*, **14** (2002), no. 1, 85-137.

8. S.-I. Ei, M. Mimura and M. Nagayama, Pulse-pulse interaction in reaction-diffusion systems, *Physica D*, **165** (2002), 176-198.

9. P. Gray and S. K. Scott, Autocatalytic reactions in the isothermal, continuous stirred tank reactor: oscillations and instabilities in the system A+2B→3B, B→C, **39** (1984), 1087-1097.

10. Y. Hayase and T. Ohta, Sierpinski gasket in a reaction-diffusion system, *Phys. Rev. Lett.*, **81** (1998), 1726-1729.

11. S. Kondo, R. Asai, A reaction-diffusion wave on the skin of the marine angelfish Pomacanthus, *Nature*, **376** (1995), 765-768.

12. K. J. Lee, W. D. McCormick, J. E. Pearson and H. L. Swinney, Experimental observation of self-replicating spots in a reaction-diffusion system, *Nature*, **369** (1994), 215-218.

13. K. Lust, Improved numerical Floquet multipliers, *Int. J. Bifurcation and Chaos*, **11** (2001), no. 9, 2389-2410.

14. H. Meinhardt, *The Algorithmic Beauty of Sea Shells*, Springer, 2003.

15. M. Mimura and M. Nagayama, Nonannihilation dynamics in an exothermic reaction-diffusion system with mono-stable excitability, *Chaos*, **7** (1997), 817.

16. Y. Morita and H. Ninomiya, Entire solutions with merging fronts to reaction-diffusion equations, *J. Dyn. Diff. Eqs.*, **18** (2006), 841-861.

17. S. Nasuno, Dancing "atoms" and "molecules" of luminous gas-discharge spots, *Chaos*, **13** (2003), 1010.

18. Y. Nishiura, T. Teramoto and K.-I. Ueda, Scattering and separators in dissipative systems, *Phys. Rev. E*, **67** (2003), 056210.

19. Y. Nishiura, T. Teramoto and K.-I. Ueda, Dynamic transitions through scattors in dissipative systems. *Chaos*, **13** (2003), 962.

20. Y. Nishiura, T. Teramoto, and K.-I. Ueda, Scattering of traveling spots in dissipative systems, *Chaos*, **15** (2005), 047509.

21. Y. Nishiura and D. Ueyama, A skeleton structure of self-replicating dynamics, *Physica D*, **130** (1999), 73-104.

22. Y. Nishiura and D. Ueyama, Spatio-temporal chaos for the Gray-Scott model, *Physica D*, **150** (2001), 137-162.

23. C. P. Schenk, M. Or-Guil, M. Bode and H.-G. Purwins, Interacting pulses in three-component reaction-diffusion systems on two-dimensional domains, *Phys. Rev. Lett.*, **78** (1997), 3781-3784.

24. T. Teramoto, K.-I. Ueda and Y. Nishiura, Phase-dependent output of scattering process for traveling breathers, *Phys. Rev. E*, **69** (2004), 056224.

25. H. Yagisita, Backward global solutions characterizing annihilation dynamics of travelling fronts, *Publ. Res. Inst. Math. Sci.*, **39** (2003), no. 1, 117-164.

Graduate School of Natural Science and Technology, Kanazawa University, Kakuma-machi Kanazawa, Ishikawa, 920-1192, Japan.
E-mail: zeron_5351@yahoo.co.jp

Research Institute for Mathematical Sciences, Kyoto University, Sakyo-ku Kyoto, Kyoto, 606-8502, Japan.
E-mail: ueda@kurims.kyoto-u.ac.jp

Chitose Institute of Science and Technology, 758-65 Bibi, Chitose, Hokkaido, 066-8655, Japan.
E-mail: teramoto@photon.chitose.ac.jp

Institute of Science and Engineering, Kanazawa University, Kakuma-machi Kanazawa, Ishikawa, 920-1192, Japan. PRESTO, Japan Science and Technology Agency, 4-1-8, Honcho Kawaguchi, Saitama, 332-0012, Japan.
E-mail: nagayama@kenroku.kanazawa-u.ac.jp

Research Institute for Electronic Science, Hokkaido University, Kita 20 Nishi 8, Kita-ku, Sapporo, Hokkaido, 060-0812, Japan.
E-mail: nishiura@nsc.es.hokudai.ac.jp